Towards time-domain modelling of wheel/rail noise: Effect of the dynamic track model

Contact Mechanics and Wear of Rail/Wheel Systems (CM 2022)

Institution of MECHANICAL ENGINEERS
Journal of RAIL AND RAPID TRANSIT

Proc IMechE Part F: J Rail and Rapid Transit
2023, Vol. 0(0) 1–10

DOI: 10.1177/09544097231179514
journals.sagepub.com/home/pif
Sage

Towards time-domain modelling of wheel/rail noise: Effect of the dynamic track model

Jannik Theyssen

Abstract

Transient events in railway rolling noise, such as the characteristic impulsive noise at switches and crossings, can significantly contribute to the perceived annoyance, despite being difficult to detect in the standard frequency-domain methods to analyse rolling noise. Studying these transient effects and their perception requires predicting the noise in the time domain. While several time-domain approaches exist for predicting the dynamic interaction of wheel and rail, predicting the associated rolling noise with adequate accuracy is computationally costly. The lack of a model for transient noise and the need for studying its perception was recently identified. Aiming for a comprehensive time-domain radiation model that includes the wheel and track contributions to rolling noise, this work focuses on the track radiation. The modelling approach taken here is based on a 2.5D formulation for the acoustic radiation and moving Green's functions in the air. The computational cost, which lies mainly in the 2.5D BE calculations, is addressed by pre-calculating acoustic transfer functions. These transfer functions can be combined with different dynamic track models. Different dynamic track models in turn affect radiated sound field in different ways. Here, the sound fields produced by six different track models are compared, including different support types and analytical and numerical rail models. Several descriptors of the sound field are analysed. In terms of the radiated sound power and radiation efficiency, modelling the rail as a simple beam leads to similar results as elaborate numerical models up to about 5 kHz. In terms of the track-side sound pressure, simple beam models can provide similar results only up to 2.5 kHz. Euler-Bernoulli (E-B) beams seem unfit for time-domain predictions of the radiated noise as they over-estimate the bending wave speed at high frequencies. The results also show that the standard track decay rate (TDR) and the decay of acoustic sound pressure along the track are comparable.

Keywords

Railway rolling noise prediction, railway track, track modelling, Euler-Bernoulli beam, timoshenko beam, 2.5 D FE/BE, Green's functions, doppler shift

Date received: 9 January 2023; accepted: 3 May 2023

Introduction

Transient events in the wheel-rail contact frequently create audible and unpleasant temporal patterns in the rolling noise from railway operations. These transients can emerge from necessary features in the track, such as rail joints or switches and crossings, or defects such as wheel flats or rolling contact fatigue cracking.[1] Whichever the cause, it was shown that the presence of transients increases the perceived loudness in pass-by signals with the same equivalent sound energy level.[2] The lack of a model for transient noise and the need for studying its perception was recently identified.[1,3] Simulating pass-by noise in the presence of such events is a multi-layered task: An accurate prediction of the rolling contact forces in the time domain is needed. With the forces as the input, the resulting vibrations in the track components and wheels, and subsequently the resulting sound field need to be simulated. In that context, the superposition of all sound sources, their relative motion with respect to a stationary observer and the surrounding acoustic geometry needs to be considered. The size of this modelling task can easily lead to computationally unfeasible models.

Pieren et al.[4] present an auralization tool for railway rolling and impact noise that uses sound synthesis. The model follows a source-path-receiver concept using distributed point sources. An equivalent roughness serves as the input to a calculation of the mechanical excitation of wheel and rail. Their modal behaviour is captured in digital filters in the time domain. This results in a flexible simulation tool. However, it requires assuming linear behaviour in the wheel/rail contact, which especially for impacts can lead to large errors.[5] It is also unclear whether modelling the radiation from the rail as distributed point sources is perceptionally different from a more realistic model.

Wu and Thompson,[6] and more recently, Torstensson et al.,[3] and Nielsen et al.[1] investigate the noise from

Chalmers University of Technology, Gothenburg, Sweden

Corresponding author:
Jannik Theyssen, Division of Applied Acoustics, Chalmers University of Technology, Sven Hultins Gata 6, 41258 Gothenburg, Sweden.
Email: jannik.theyssen@chalmers.se

such impact loads in a hybrid approach. In this approach, the forces obtained in a non-linear time-domain model are transformed into the frequency domain, where vibration and noise radiation are evaluated by representing the forces as an equivalent roughness spectrum. This reduces the computational cost, however, the frequency-domain noise calculation does not allow evaluating the perception of the presence of these transients in the noise.

In this work, a modelling approach is proposed in which the complete chain of modelling tasks listed above is calculated in the time domain. The scope of this work is two-fold: Firstly, a computationally efficient method to simulate the noise caused by a vertical force passing by on a rail in the time domain is presented. The method is based on the Wavenumber domain Boundary Element Method (WBEM or 2.5D BE)[7,8] and the concept of moving Green's functions,[9,10] applied to transfer functions in air. The method is introduced in more detail in the first subsection in the following Section. The modelling approach involves calculating impulse responses of the sound pressure on track-side locations given a unit force pulse on the rail. The dynamic response of the rail and superstructure is thus an essential part of the predicted sound field.

Therefore, the dynamic model's effect for the rail and its support on the predicted sound field is investigated. This includes analytical models based on Euler-Bernoulli (E-B) beam theory and Rayleigh-Timoshenko beam theory, as, for example, used in the context of vehicle/track coupled dynamics[11] and in TWINS.[12] It also considers a more detailed, numerical modelling approach based on the Waveguide Finite Element method (WFEM or 2.5D FE).[8,13] Further, different rail support models are researched, including free rails, continuous supports, and systems with discrete support points along the track incorporating sleeper masses. The consequences of the dynamic track model for the properties of the acoustic sound field are discussed in discussed in the results section, including the radiated sound power, the radiation ratio, the directivity in the track cross-section, the sound pressure impulse response at different positions along the track, the decay of acoustic sound pressure along the track. A demonstration of the Doppler effect during a pass-by is included.

The conclusion section provides guidelines for choosing a dynamic track model depending on the desired application and required information. The last section gives an outlook on possible further research.

Method

Pass-by via acoustic moving Green's functions

The starting point is a formulation of the dynamic response and the sound radiation in the wavenumber-frequency domain. This means that wave propagation along the direction of the track is assumed both in the structure and the surrounding fluid. The cross-section is assumed constant in this direction. The details of this approach are presented in a parallel work[14] and are therefore only briefly summarised here. Figure 1 indicates this part by a dotted line. It consists of the following steps:

1. The dynamic response on the surface of the structure to a harmonic unit force excitation is expressed in terms of the transfer functions $H_d(f, k, y, z)$. To establish these transfer functions, different track models can be utilised based, e.g., on E-B beam theory or numerical methods like the Waveguide Finite Element Method (WFEM).[8,13]
2. The acoustic transfer functions $H_a(f, k, y, z)$, describing the wavefield along the track in a certain receiver location (y_r, z_r) perpendicular to the track due to the vibration of the node (y_s, z_s) on the boundary Γ, are pre-calculated using the WBEM.[7,8]
3. Multiplying $H_a(f, k, y, z)$ and $H_d(f, k, y, z)$ and integrating over the boundary Γ of the vibrating structure finally produces the transfer functions $H_{da}(f, k)$ which describe the acoustic field at the location (y_s, z_s) in the form of plane waves along the track for a harmonic unit force on the rail.

Having access to such transfer functions and given a series of rolling contact forces $F(x, t)$, the radiated sound field can be efficiently calculated in any receiver position along the track.

For obtaining the pressure signals, two different paths could be followed. Either the forces are also transformed to the wavenumber-frequency domain and multiplied with the

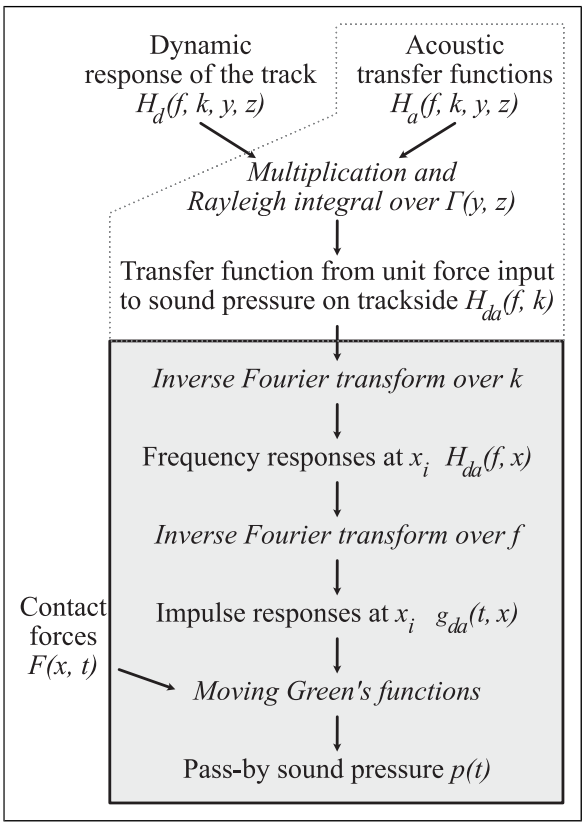

Figure 1. Algorithm for calculating the pass-by sound pressure. This work focuses on the shaded rectangle.

transfer functions $H_{da}(f, k)$. Then, a 2D inverse Fourier transform back to time and space will give the desired pressure signals. Alternatively, from $H_{da}(f, k)$ so-called moving Green's functions can be obtained which then can be convolved with the time signal of the contact forces. This process is chosen here (shown in the shaded part of Figure 1) as it has advantages with respect to computational efficiency and memory consumption.

To obtain the moving Green's functions, the pressure transfer function to a receiver position (x_r, y_r, z_r) is evaluated for a force excitation pulse at K linearly spaced positions on the rail, with the spacing $\mathrm{d}x = v\mathrm{d}t = v/f_s$, the vehicle speed v and the desired sampling frequency f_s. The impulse responses are collected in the Green's function matrix $g_{da}(t, x)$. If the rail support is continuous, only the absolute distance between the excitation and the receiver is relevant, which makes it possible (and computationally more efficient) to excite at the position x_0 and evaluate the acoustic impulse responses at linearly spaced locations along the rail. For a discretely supported track, the excitation position relative to the sleepers is relevant and the computational effort is somewhat increased. In the following, impulse responses are generated for eight excitation positions in a sleeper bay and interpolated for positions in between.

Figure 2 visualises the principle for computing the pass-by sound pressure given the Green's function matrix $g_{da}(t, x)$, the vehicle speed v and the rolling contact force defined in space and time $F(x, t) = F(t)\delta(x - vt)$.[9,10] The diagonal curves represent peaks in the calculated impulse responses. The slope of these curves in the left figure is determined by the phase speed c of the waves in the rail. Aligning the Green's functions with the corresponding force location, at each time step, results corresponds to a shearing of the Green's function matrix as seen in the right figure. The total sound pressure at location x_0 and time step t_n is then calculated as

$$p(t_n) = \sum_{i=0}^{K} g_{da}\left(i\Delta x, t_n - \frac{i\Delta x}{v}\right) F\delta(i\Delta x)\Delta x \qquad (1)$$

with $g_{da}(x, t < 0) := 0$. Notice that this formulation includes the Doppler effect, not due to the relative motion between source and observer (the rail and the receiver are stationary), but instead because of compression or elongation of the waves in the rail due to the time-dependent excitation. The Doppler shift is here described by $f = (1 + v/c)f_0$ with f and f_0, the observed and original frequency, respectively. The transfer functions to the spectra and impulse responses along the track are investigated in the following.

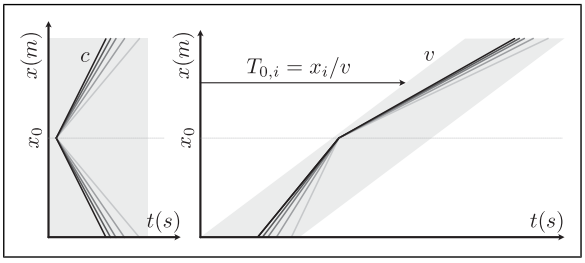

Figure 2. Algorithm for computing the pass-by pressure in a stationary position via moving Green's functions. Left: Impulse response matrix $g_{da}(x, t)$, where diagonal lines indicate the arrival of wavefronts at x_0 for a force excitation pulse at x. Right: Aligning the impulse responses with the location of the moving excitation force in space and time.

Description of the track models

Six different rail models, labelled R1 to R6, are used to calculate the input velocity for the radiation calculation.

The models increase in complexity in both the rail model and their supports. All models are designed to represent the dynamic behaviour of a UIC60 rail. Their parameters are summarised in Table 1. The first two rails are based on E-B beam theory, the first being freely suspended and the second on a continuous, single-layer support.[15] The third rail model is based on Rayleigh-Timoshenko (R-T) beam theory, with discrete rail seats and a two-stage support including sleepers. This way, the dynamic response of the ground, the sleeper mass and the rail pad can be included, as well as effects due to the discrete support.[15–17] The fourth to sixth rail models are using the waveguide Finite element method for calculating the dynamic response of the rail. In this formulation, multiple wave types are included in the calculation, the surface velocities at each point on the boundary of the rail can be predicted in all directions, and cross-coupling between the vertical and horizontal directions is included.

In the FE-based rail models, two nodes on the rail head can be used as excitation nodes, where one is located on the symmetry axis and the other one is off the symmetry axis by 1 cm. The nodes across the rail foot are coupled to a spring-mass-spring system in the discretely supported case, similar to model R3. As in the three cases above, the rail is modelled freely suspended, on a continuous support, and on a discrete support, producing setups R4, R5, and R6, respectively. The model R6 is connected to the support in five nodes across the rail foot. A rail inclination is not considered here.

In all cases, only the velocity of the rail is considered in the radiation model, and vibrations of sleepers or slabs are neglected. The velocity on the surface of the rail cross-section is mapped to the boundary of the radiation model for a rail. The beam models do not consider cross-sectional deflections and so the same vertical velocity is applied in every node of the same boundary. Acoustically, the rail is situated 5 cm above a hard ground. All calculations are carried out with acoustic transfer functions for this case, except for the calculation of the directivities, which for demonstration uses the acoustic transfer functions of the rail in free space.

Results

Receptances

The vertical track receptance of the included track setups is presented in Figure 3. The receptance of the two free rails R1 and R4 follow the expected slope with bending waves in

a beam up to about 1.2 kHz, above which the WFE-based rail diverges due to the onset of further wave types. The single-stage continuous support models R2 and R5 have a resonance at about 300 Hz, above which the receptance of the beam model R2 tends towards that of the free beam R1 while the WFE-based model shows a similar behaviour as the unsupported WFE model R4. This indicates that the influence of the track support decreases at higher frequencies. The two-stage, discretely supported rail models R3 and R6 show two resonances at 125 Hz and 310 Hz, respectively, corresponding to the resonances of the sleepers and the cut-on of the vertical bending wave. The discrete support further gives rise to the pinned-pinned mode at about 1.1 kHz, where the bending wavelength is twice the sleeper spacing, and at other frequencies at which the sleeper spacing is a whole number multiple of the vertical bending wavelength.

Radiation ratio and sound power

The radiation ratio σ is calculated by normalizing the radiated sound power by the average surface velocity.[8] No significant influence of the type of rail support or rail model is observed, as the radiation ratio is mainly a consequence of the acoustic transfer function from the structure.

In contrast, the radiated sound power itself is strongly dependent on the rail support. Figure 4 compares the sound power level (L_W) radiated from the beam and the WFE-based models, for vertical unit force harmonic excitation. In each comparison, the WFE-based model is excited both centrally and in the position off the symmetry axis. The shaded area indicates the 3 dB margin. Especially for the central excitation of the rail, the beam models provide decent estimates of the L_W up to 3 kHz (5 kHz for the Timoshenko-beam model). For an asymmetric excitation, the beam models tend

Table 1. Parameters for the rail models.

		R1	R2	R3	R4	R5	R6
		Euler-Bernoulli	Euler-Bernoulli	Rayleigh-Timoshenko	WFE	WFE	WFE
Model Support		Free	Continuous	Discrete	Free	Continuous	Discrete
Rail							
bending stiffness EI	MN m^2	6.42	6.42	6.42			
mass* m'	kg/m	60	60	60			
Young's modulus E_r	GPa				210	210	210
shear stiffness GA	MN			617			
shear parameter κ_r	–			0.4			
rotational inertia ρI	kg m^4			0.24			
density ρ	kg/m^3				7850	7850	7850
Poisson ratio ν	–				0.3	0.3	0.3
damping loss factor η_r	–	0.001	0.001	0.001	0.001	0.001	0.001
Pad							
vert. stiffness* s_v'	MN/m^2		217				
vert. stiffness s_{pv}	MN/m			130			130
vert. damping loss factor η_{pv}	–		0.25			0.25	
lat. stiffness s_{pl}	MN/m						14
lat. damping loss factor η_{pl}	–					0.1	
Young's modulus E_p	MPa					16	
Poisson ratio ρ_p	–					0.3	
Ballast							
vert. stiffness s_{bv}	MN/m			100			100
vert. damping loss factor η_{bv}	–			0.5			0.5
lat. stiffness s_{bl}	MN/m						100
lat. damping loss factor η_{bl}	–						0.05
Sleeper							
Mass m_s	Kg						
Spacing d_s	M						
Count n_s	–						

* per unit length

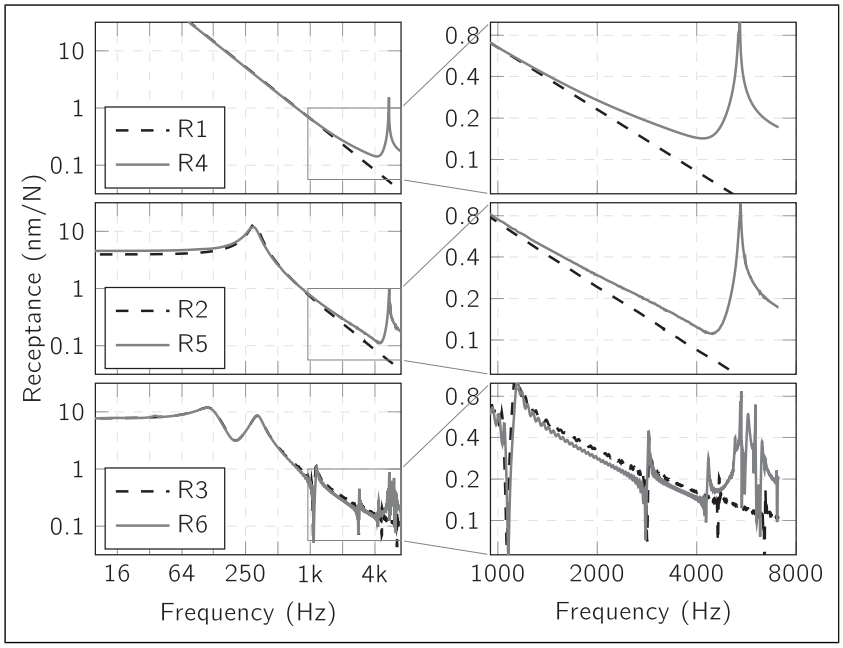

Figure 3. Vertical receptance of the track models, compared per support type, with symmetric excitation on the rail head.

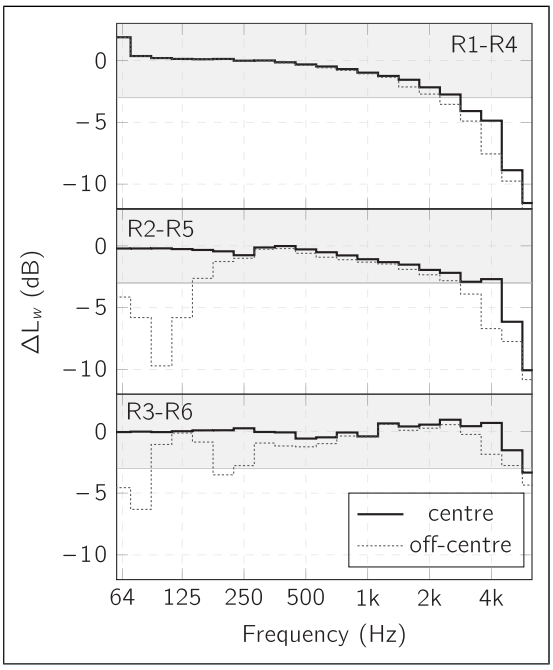

Figure 4. Difference of the radiated sound power for harmonic unit excitation, from beam and WFE-based rail models, per support type.

to under-estimate L_W. For low frequencies, this occurs especially in the frequency region of the lateral bending wave. The software package TWINS[12] introduces a second bending beam as a sound source to compensate for this. At high frequencies, several different wave types contribute to the vibration, leading to a general underestimation of the radiated L_W compared to the WFE model.

Cross-sectional directivity

For brevity, only the two discretely supported track models, R3 and R6, are included in the discussion of the directivity. About 50 receivers are arranged in a half-circle with 20 m radius around a rail in acoustic free space. The angle between the horizontal plane and a vector from the rail to the receiver is indicated on the y-axes in Figure 5, i.e., horizontal radiation to the right is plotted at 0 rad, vertical upward radiation at $\pi/2$ rad, and $-\pi/2$ rad describes a receiver position below the rail. The figures show the difference in sound pressure level, in 1/3-octave bands, that the two dynamic track models produce in each receiver point.

Impulse responses along the track

Impulse responses of the sound pressure along the track can be calculated by inverse Fourier transform over the frequency domain. Here, the impulse responses are evaluated in a line of receiver positions, 7.5 m from the track centre and 1.2 m above the top of the rail as shown in Figure 6. The hammer symbol represents the unit force excitation pulse on the rail.

Figure 7 shows impulse responses along the track for a pulse force on the top of the rail at position 0 m, for different track setups. The initial 20 ms delay is due to the distance of the receiver from the rail. It is visible that in all figures, the impulse arrives later for larger distances due to the velocity of the bending waves in the rail. This frequency-dependent velocity of the waves also leads to dispersion, with high-frequency waves arriving first.

The impulse responses calculated with the track model R3 are rather short, decaying by 30 dB in about 20 ms. Below 2 m, the impulse is much shorter, and the peak level is not as high. This is because bending waves radiate sound waves at an angle different from zero degrees (i.e., perpendicular), and thus the sound waves are directed away from the excitation position. The WFE-based models show a more complex pattern in the impulse responses along the track, which are likely a result of the combined radiation of the several wave types included in the models. The free rail model R4 produces much longer impulse responses,

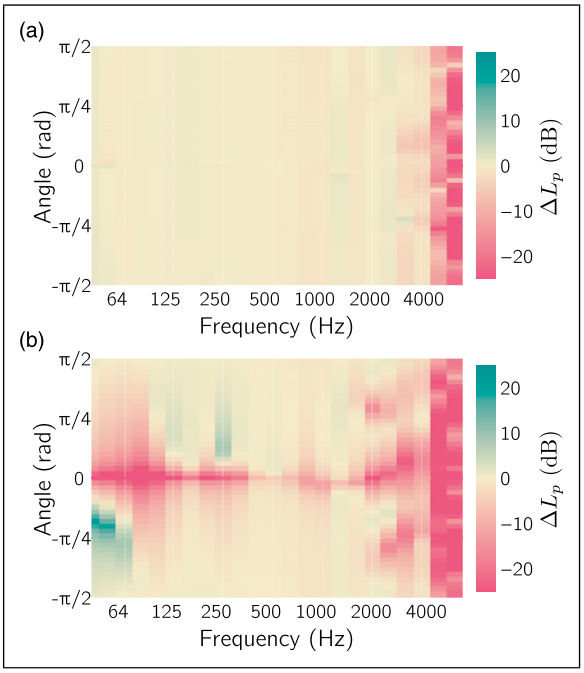

Figure 5. Comparison of the directivity of R6 to R3 for (a) central and (b) off-centre excitation.

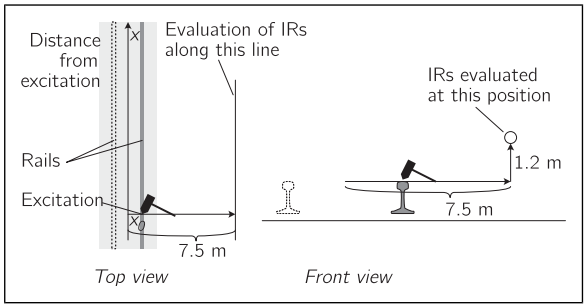

Figure 6. Evaluation position of the impulse responses along the track.

increasing in length at a larger distance. The long response can be attributed to the missing coupling of the rail to the ground which would lead to energy leakage, as the comparison to the continuously supported rail R5 shows. Impulse responses from the discretely supported WFE-rail R6 are similar to that of the discretely supported beam in that the main part of the impulse decays within about 20 ms. It is further noticeable that receivers closer to the excitation point give larger levels compared to the discretely supported beam model R3.

The white, diagonal lines indicate the travel time of a wave in air that is excited simultaneously to the impact on the rail. It is clear that at $x = 0$ *m*, this time is identical to the simulation. At larger distances, the first wave fronts radiated from the rail arrive earlier. This indicates that each impulse response is dominated by the radiation from the section of rail closest to the receiver, and not by rail section close to the excitation point. Representing the radiation from the rail as a point source can not capture this behaviour.

The temporal structure of the impulse responses created by the different rail models is further investigated in Figure 8. Here, the pressure response at $x = 1$ m from the excitation position is compared to the impulse at $x = 64$ m distance,

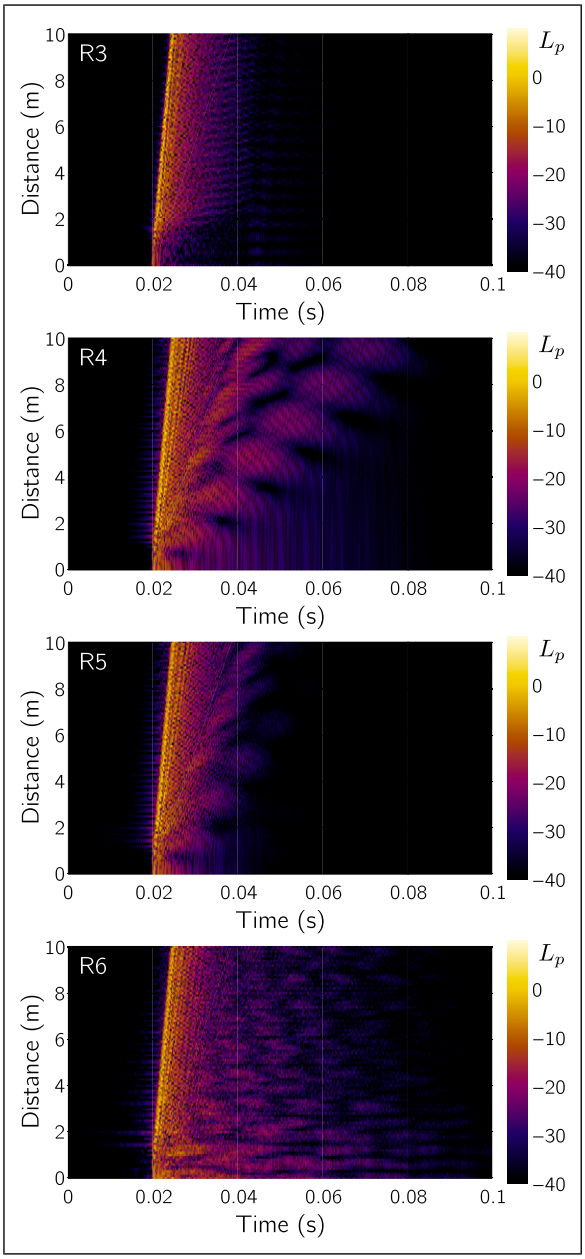

Figure 7. Predicted impulse response magnitude (dB re. 20 μ Pa) along the track for a force pulse on the rail head at t = 0 s, x = 0 m. The white lines indicate the travel time of a wave in air from the excitation point to each receiver.

per track support type, still for the receiver located at $(y, z) = (7.5\text{ m}, 1.2\text{ m})$. While the timing of the first wavefront is almost identical for all six track models at 1 m, the models R1 and R2 produce peaks significantly earlier at larger distances. This is likely due to the inherent approximations of the Euler-Bernoulli beam theory, which leads to an overestimation of the wave speed at higher frequencies. The track support does not seem to influence the timing of the first wave front but instead shapes the decay of the impulse responses as different waves might have different decay rates.

Track decay rate and acoustic spatial decay

The frequency composition of the sound field along the track for a harmonic force excitation on the rail is investigated in this section. Figure 9 visualises the sound

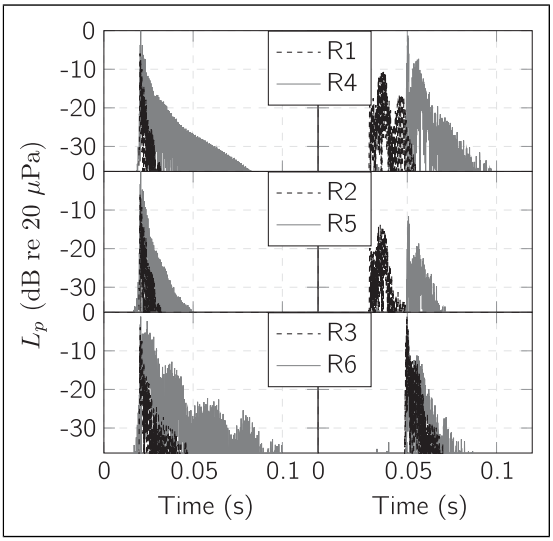

Figure 8. Impulse responses predicted at 1 m (left) and 64 m (right) distance from the excitation position.

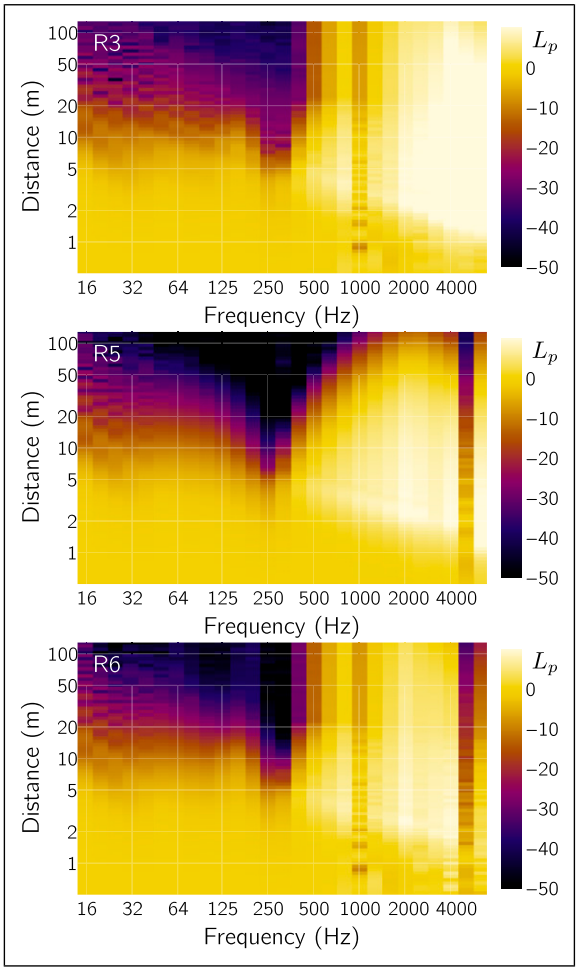

Figure 9. 1/3-octave band response magnitude in dB along the track for harmonic unit excitation at x = 0 m. Each 1/3-octave band is normalised to L_p at 0 m.

pressure data in 1/3-octave band spectra for logarithmically increasing distances and for three different track setups. The sound pressures in each 1/3-octave band have been normalised with the band pressure at 0 m. In all

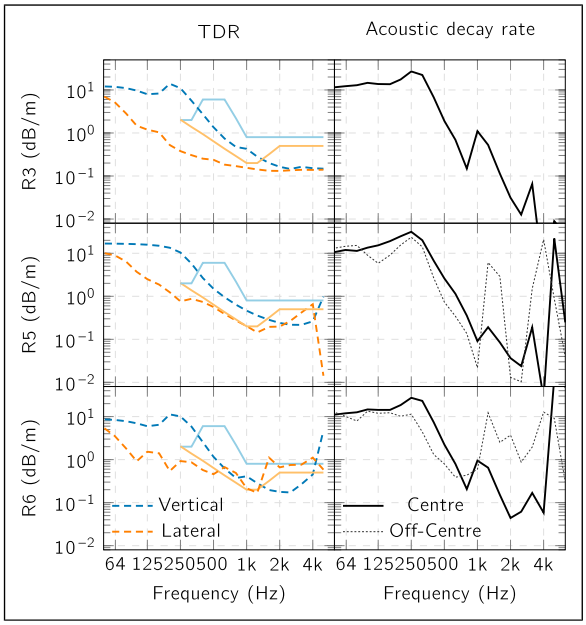

Figure 10. Vertical and lateral track decay rate compared to the decay of the sound pressure level on the track side.

setups, the highest sound pressure levels are found above 1 kHz and between 1 m and 10 m from the excitation position.

This distance is related to the angle under which sound is radiated from bending waves. This angle is frequency dependent.[15] Between 200 Hz and 500 Hz, the sound pressure level drops by 20 dB within about 10 m, while the decay is less pronounced in other frequency regions. The steep decay is related to the vertical resonance of the rail on its support (see also Figure 3), where vibrational energy is effectively dissipated in the rail pads. The characteristics of the decay of the two discretely supported tracks R3 and R6, respectively, are similar up to 4 kHz. It has been shown that the continuous support of a rail can reduce its noise emissions.[15,17] This is also seen in the comparatively stronger decay of the sound pressure along the rail above 500 Hz for track R5.

A standardised way to describe the vibrational decay along the track is the track decay rate (TDR) according to EN-15461,[18] taking the input- and transfer accelerance to several positions on the rail as the input. The decay rate is then calculated based on the ratio of the transfer accelerances to the input accelerance, scaled with the distance. An analogous quantity is calculated here, using the squared pressure on the trackside instead of the accelerance, here termed "acoustic decay rate".

Figure 10 compares the vertical and lateral (structural) TDR of three track models the acoustic decay rate, for both a centre and an off-centre excitation of the rail. The TSI limit curves for the TDR are included for orientation. For comparability, the acoustic decay rate has been scaled to align its y-axis range with the TDR. For the symmetric excitation, the acoustic decay along the track has a similar shape as the vertical TDR, for all tracks. The off-centre excitation in the WFE rails leads to a higher decay in the frequency range above 1 kHz. Further investigation of the relation between the acoustic decay and the vertical

and lateral TDR is suggested, especially for different asymmetric excitation and for high frequencies, but this is outside the scope of this work.

Pass-by sound pressure in time-domain

As a demonstration of the method, the sound pressure level in a stationary point during the pass-by of a force on the rail is presented below. A time-domain simulation of the rolling contact force is carried out in the in-house software WERAN[10] with a vehicle speed of 100 km/h and the measured roughness profiles of wheel and rail. WERAN combines precalculated impulse response functions of the track and wheels with a transient rolling contact model.[19,20] The impulse response functions of the wheel include its modal behaviour as well as the primary suspension. The rail roughness measurement was carried out on a German high-speed line,[21] and the wheel roughness was measured on a French freight wagon.[22] The total length of the pass-by is 3 s or about 81 m. The sound pressure in a stationary microphone position was then calculated via Green's functions as described above.

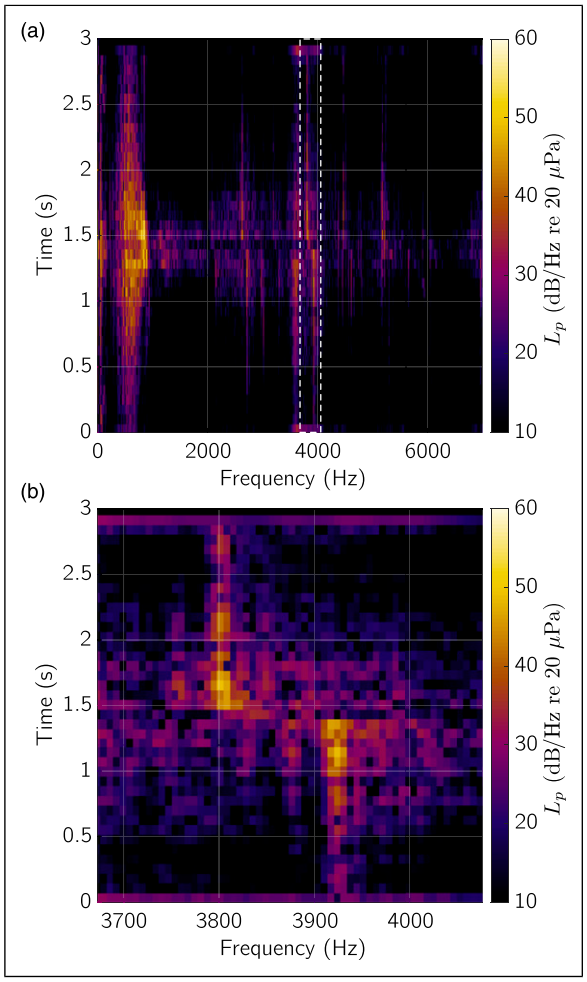

Figure 11. (a) Spectrogram of the pass-by noise produced by a simulated contact force moving over a discontinuously supported, WFE-based track. (b) Doppler effect due to the moving contact force and the wave speed in the rail.

The spectrogram of the resulting sound pressure signal is presented in Figure 11. The stationary microphone is passed at about 1.5 s. The largest sound pressure levels are observed in frequency range between about 100 Hz and 1000 Hz. However, some distinct frequency components can be found up to 5 kHz. These are likely related to dynamic resonances in the wheel or the track, since the roughness spectrum does not contain such strong tonal components. The bottom figure shows one of these frequency lines and shows the effect of the Doppler shift during the pass-by. From the observed frequency shift of a bit more than 100 Hz and the known vehicle speed of 100 km/h, the corresponding sound speed is found to be about 1750 m/s, which matches the expected phase velocity of vertical bending waves in a free rail.

Conclusions

A method to predict the sound radiation from track vibrations in the time domain via acoustic moving Green's functions has been presented. An efficient prediction of the sound field around the track is achieved by precalculating impulse response functions that describe the acoustic transfer from the track surface to receiver points in the field. This way, a high frequency, physical prediction of the pass-by noise from vibrating railway track is possible in under 1 hour on a computer with a 3.5 GHz Dual-Core processor and 16 GB memory. The proposed time-domain approach includes the non-linear behaviour of the rolling contact while also allowing predicting the pressure signal at a stationary receiver position. By describing the radiation from the rail via acoustic impulse responses, its complex radiation behaviour can be efficiently captured without assuming equivalent sources.

Table 2. Guidelines for selecting a dynamic track model suggesting range of validity with respect to frequency.

	Euler-Bernoulli	Rayleigh-Timoshenko	WFEM
Sound power	≤2.5 kHz	≤5 kHz (symmetric excitation), ≤4 kHz (asymmetric excitation)	≤7 kHz
Radiation ratio	≤7 kHz	≤7 kHz	≤7 kHz
Cross-sectional directivity	≤1.5 kHz	≤4 kHz (symmetric excitation) ≤2.5 kHz (asymmetric excitation)	≤7 kHz
Directivity along the track	≤1.5 kHz	≤4 kHz	≤7 kHz
Arrival time of the pressure signal at short distances	Comparable to WFEM	Comparable to WFEM	Reference
Arrival time of the pressure signal at large distances	Too early compared to WFEM	Comparable to WFEM	Reference
Complexity of the time signal	Less detailed compared to WFEM	Less detailed compared to WFEM	Reference

The performance of six dynamic track models was compared in terms of predicting the radiated sound field and several derived quantities in the frequency- and the time domain. The results indicate the applicability of different models depending on the scope of the simulations.

Regarding the frequency domain quantities,

- It is found that the rail models based on the E-B beam theory provide similar results to the more complex WFE-based rail models up to 2.5 kHz in terms of predicting the radiated sound power, while the rail based on Timoshenko beam theory matched the WFE rail up to 5 kHz for a symmetric excitation. An asymmetric excitation leads to an underestimation of the radiated sound power above 4 kHz and around the resonance frequency of the lateral bending wave between 60 Hz and 100 Hz.
- No significant differences between the tracks are observed for the radiation ratio, even for the (dynamically) free rail models.
- An analysis of the directivity shows a high agreement of the Timoshenko-beam model to the WFE model for symmetric excitation up to 4 kHz, but larger differences in the horizontal plane for an off-centre excitation.
- The spatial decay of acoustic sound pressure along the track is analysed in 1/3-octave bands. Similar decay rates are found for the rail based on the Timoshenko beam theory and the WFE rail.
- The acoustic decay over frequency is found qualitatively similar to the standard vertical (structural) TDR, at least for vertical excitation of the track. The discretely supported Timoshenko beam again produces similar results as the WFE formulation up to 4 kHz. Further investigations are possible.

Regarding the time domain quantities,

- The calculated acoustic impulse responses are typically rather short, decaying about 30 dB in 20 ms for all tracks.
- The first wavefront of the impulse response arrives significantly earlier when using E-B beam theory to model the rail, likely due to the overestimation of the high-frequency bending wave stiffness and the corresponding higher bending wave speed. A Timoshenko-beam or WFE-based rail model should be favoured for time-domain applications aiming for auralisation.
- The dispersion of the waves, observable as a widening of the impulse response over distance, shows fairly large differences between the Timoshenko beam and the WFE rail. Since this difference does not seem to affect the radiated sound power, it should be investigated if this difference is relevant to human perception.

Based on the comparison of the effect of different dynamic track models on the produced sound field, guidelines for the selection of the dynamic track model are derived. These assume the employment of an adequate radiation model based on the 2.5D BE method that incorporates the surface geometry of the rail. These guidelines are summarised in Table 2.

Outlook

Even though the method is based on established calculation approaches such as moving Green's functions and the Wavenumber Boundary Element method, a validation of the complete modelling chain would be desirable and has not yet been carried out. The beam models only consist of a single beam moving in the vertical direction (unlike in TWINS, where a vertical and a lateral beam are included and coupled by an empirically derived factor). Even though including a second beam likely does not increase the upper-frequency limit, it might mitigate some of the shortcomings observed in the below 100 Hz, which could be investigated in future work. Perceptive differences between different dynamic rail models could be evaluated in a future study. Finally, the presented approach can be utilised to auralising the sound radiated by railway tracks for researching the human response to transient events in the pass-by noise of railway vehicles.

Declaration of conflicting interests

The author(s) declared no potential conflicts of interest with respect to the research, authorship, and/or publication of this article.

Funding

The author(s) disclosed receipt of the following financial support for the research, authorship, and/or publication of this article: The current study is part of the ongoing activities in CHARMEC – Chalmers Railway Mechanics (www.charmec.chalmers.se). Parts of the study have been funded from the European Union's Horizon 2020 research and innovation programme in the In2Track3 project under grant agreements No 101012456. The computations were enabled by resources provided by the Swedish National Infrastructure for Computing (SNIC), partially funded by the Swedish Research Council through grant agreement no. 2018-05973.

ORCID iD

Jannik Theyssen https://orcid.org/0000-0001-6041-0763

References

1. Nielsen JCO, Pieringer A, Thompson DJ, et al. Wheel–rail impact loads, noise and vibration: a review of excitation mechanisms, prediction methods and mitigation measures. In: Degrande G, Lombaert G, Anderson D, et al. (eds). *Noise and vibration mitigation for rail transportation systems, volume 150*. Cham: Springer International Publishing, pp. 3–40.
2. Kaku J and Yamashita M. Impact noise from railroads. *J Sound Vib* 1988; 120(2): 333–337.
3. Torstensson P, Squicciarini G, Krüger M, et al. Wheel–rail impact loads and noise generated at railway crossings – influence of vehicle speed and crossing dip angle. *J Sound Vib* 2019; 456: 119–136.
4. Pieren R, Heutschi K, Wunderli JM, et al. Auralization of railway noise: emission synthesis of rolling and impact noise. *Appl Acoust* 2017; 127: 34–45.

5. Pieringer A, Kropp W and Nielsen JCO. The influence of contact modelling on simulated wheel/rail interaction due to wheel flats. *Wear* 2014; 314(1): 273–281.
6. Wu TX and Thompson DJ. A hybrid model for the noise generation due to railway wheel flats. *J Sound Vib* 2002; 251(1): 115–139.
7. Duhamel D. Efficient calculation of the three- dimensional sound pressure field around a noise barrier. *J Sound Vib* 1996; 197(5): 547–571.
8. Nilsson CM, Jones C, Thompson D, et al. A waveguide finite element and boundary element approach to calculating the sound radiated by railway and tram rails. *J Sound Vib* 2009; 321(3): 813–836.
9. Nordborg A. Wheel/rail noise generation due to nonlinear effects and parametric excitation. *J Acoust Soc Am* 2002; 111(4): 1772–1781.
10. Pieringer A, Kropp W and Thompson DJ. Investigation of the dynamic contact filter effect in vertical wheel/rail interaction using a 2D and a 3D non-hertzian contact model. *Wear* 2011; 271(1): 328–338.
11. Zhai W, Wang K and Cai C. Fundamentals of vehicle–track coupled dynamics. *Veh Syst Dyn* 2009; 47(11): 1349–1376.
12. Thompson D, Hemsworth B and Vincent N. Experimental validation of the TWINS prediction program for rolling noise, part 1: description of the model and method. *J Sound Vib* 1996; 193(1): 123–135.
13. Theyssen JS, Aggestam E, Zhu S, et al. Calibration and validation of the dynamic response of two slab track models using data from a full-scale test rig. *Eng Struct* 2021; 234: 111980.
14. Theyssen J, Pieringer A and Kropp W. Efficient calculation of the three-dimensional sound pressure field around a railway track. Manuscript, https://research.chalmers.se/en/publication/530940
15. Thompson DJ. *Railway noise and vibration: mechanisms, modelling and means of control*. 1st ed. Amsterdam: Elsevier.
16. Zhang X, Thompson DJ, Li Q, et al. A model of a discretely supported railway track based on a 2.5d finite element approach. *J Sound Vib* 2019; 438: 153–174.
17. Theyssen JS, Pieringer A and Kropp W. The influence of track parameters on the sound radiation from slab tracks. In: Degrande G, Lombaert G, Anderson D, et al. (eds). *Noise and vibration mitigation for rail transportation systems, volume 150*. Cham: Springer International Publishing, pp. 90–97.
18. EN 15461. *Railway applications - noise emission - characterisation of the dynamic properties of track sections for pass by noise measurements*, 2008.
19. Pieringer A. A numerical investigation of curve squeal in the case of constant wheel/rail friction. *J Sound Vib* 2014; 333(18): 4295–4313.
20. Kalker JJ. *Three-dimensional elastic bodies in rolling contact. Vol. 2 of solid mechanics and its applications*. Dordrecht: Springer Netherlands, 1990.
21. Thompson D, Squicciarini G, Zhang J, et al. Assessment of measurement-based methods for separating wheel and track contributions to railway rolling noise. *Appl Acoust* 2018; 140: 48–62.
22. Delavaud V. *Modélisation temporelle de l'interaction roue/rail pour une application au bruit de roulement ferroviaire*. Doctoral thesis. Paris: ENSTA ParisTech, 2011.